J. Mod. Transport. (2014) 22(1):37–44
DOI 10.1007/s40534-014-0035-1

JMT
www.springer.com/40534

Structure and properties of CIGS films based on one-stage RF-sputtering process at low substrate temperature

Yong Yan · Shasha Li · Yufeng Ou · Yaxin Ji · Chuanpeng Yan · Lian Liu · Zhou Yu · Yong Zhao

Received: 18 November 2013 / Revised: 17 January 2014 / Accepted: 18 January 2014 / Published online: 23 February 2014

Abstract Currently, Nanjing South Railway Station planning to implement slate roof renovation is integrating solar cell modules into traditional roof materials to generate clean energy. Copper–indium–gallium diselenide ($CuIn_{1-x}Ga_xSe_2$, CIGS) is one of the most promising materials for thin film solar cells. $Cu(In_{1-x}Ga_x)Se_2$ films were deposited by a one-step radio frequency magnetron sputtering process at low substrate temperature. X-ray diffraction, Raman, scanning electron microscopy, energy-dispersive X-ray spectroscopy, and electrical and optical measurements were carried out to investigate the deposited films. The results reveal that a temperature of 320 °C is critical for near-stoichiometric CIGS films with uniform surface morphology. Cu-rich phase particulates are found at less than this temperature. The sample deposited at 380 °C gives well-crystalline single-phase CIGS film. Furthermore, the electrical and optical performances of the absorber layer are improved significantly with the increasing substrate temperature.

Keywords CIGS · Low-temperature · Electrical and optical properties

Y. Yan · S. Li · Y. Ou · Y. Ji · C. Yan · L. Liu · Z. Yu (✉) · Y. Zhao
Superconductivity and New Energy R&D Center (SNERDC), School of Electrical Engineering, Key Laboratory of Advanced Technology of Materials, Ministry of Education of China, Southwest Jiaotong University, Chengdu 610031, China
e-mail: solarcells@126.com

Y. Yan
e-mail: yanyong5305@126.com

Y. Zhao
School of Materials Science and Engineering, University of New South Wales, Sydney, NSW 2052, Australia

1 Introduction

Currently, solar panels cover the majority of the railway station roofs and are capable of providing 7.17 MW (megawatt) of electricity in Nanjing South Railway Station. More and more stations planning to implement slate roof renovation are integrating solar cell modules into traditional roof materials to generate clean energy. This system is expected to be widely adopted in the near future because it promotes the effective use of platform roof space, which occupies a substantial part of a station.

Materials for efficient solar cells must have characteristics matched to the spectrum of the available light. Light-absorbing materials can often be used in multiple physical configurations to take advantage of different light absorptions and charge separation mechanisms.

Copper–indium–gallium diselenide ($CuIn_{1-x}Ga_xSe_2$, CIGS) is one of the most promising materials for thin film solar cells due to its near-optimum band gap, high optical absorption coefficients, and long-term-stability [1]. High-efficiency CIGS devices were prepared at high substrate temperatures (T_{sub}) of >550 °C, which is close to the softening temperature of the soda-lime glass (SLG) substrates [2, 3]. Therefore, deformation of glass substrate and high manufacturing costs are incurred. In contrast to the above, CIGS films fabricated by low-temperature-deposition processes (LTDPs) are more attractive for mass production. This can not only reduce the thermally induced stress on the substrate, but also offer the feasibility for flexible CIGS solar cells on polymer sheet [4]. At present, several studies have also reported on the properties and device performances of CIGS films prepared by LTDPs through three-stage co-evaporation processes [4–6]. Success of the co-evaporation method strongly depends on the precise control of each individual elemental flux

throughout the fabrication process. This is a critical challenge for large-scale mass manufacture. Recently, efforts have been made to fabricate CIGS layers by sputtering. To further reduce the fabrication costs, a one-step sputtering has been developed [7–10] to deposit CIGS films without selenization. Frantz et al. [7] prepared CIGS solar cell with an efficiency of up to 8.9 % through one-step radio frequency (RF) sputtering at T_{sub} of 550 °C. Therefore, the validity of one-step sputtering CIGS films at low T_{sub} needs to be investigated.

In our previous study [10], we reported on the effect of T_{sub} on the CIGS film properties and found that a T_{sub} of 350 °C produces a single chalcopyrite phase CIGS film. Unfortunately, all the 80 W-deposited films are deficient in Se due to Se's re-evaporation, and thus unsuitable for absorber layers. In another study [11], we demonstrated that the films sputtered at high power do not show Se's re-evaporation in the annealing process. Given all this, we improved the sputtering power from 80 to 100 W to get high-quality absorber layers and systematically investigated the structure and properties of CIGS films fabricated at less than 380 °C in this study. XRD, SEM, Raman, optical and electrical measurements were carried out to gain a better understanding of the relation between T_{sub} and the film properties.

2 Experimental details

CIGS thin films were deposited by a one-step RF magnetron sputtering process. SLG substrates with the dimensions of 2.5 cm × 2.5 cm × 1 mm were used as substrate. Before deposition, the glass substrates were ultrasonically cleaned sequentially with acetone, alcohol, and deionized water. A single ceramic quaternary $Cu(In_{0.7}Ga_{0.3})Se_2$ target with the composition of Cu, In, Ga, and Se = 25, 17.5, 7.5, and 50 atom percent ratio (at.%), respectively, was used as sputtering source. CIGS films were sputtered at the power of 100 W. Sputtering was performed in a high-purity argon atmosphere at a pressure of 0.5 Pa and an argon flow rate of 20 sccm. To calibrate the real sample temperature and the shown T_{sub}, a second thermocouple was mounted in the front side of SLG. Based on this calibration, the T_{sub} was maintained at different temperatures of 200, 260, 320, and 380 °C,. The total deposition time of the films is 120 min.

The crystallinity of the films was measured by glancing incidence X-ray diffraction with the glancing angle of 0.5° (GIXRD, PANalytical X'Pert PRO, CuKα radiation). Compositions of the films were determined by energy dispersive X-ray spectroscopy (EDS, INCA spectrometer) at an accelerating voltage of 10 keV. The accelerating voltage of 10 keV was used to give lower penetration depth-work nearer the surface of the samples. The penetration depth calculated by Monte Carlo simulation was approximately 300 nm. Surface morphologies and cross-sectional images were obtained by scanning electron microscopy (SEM, JOEL FESEM 7001). Optical transmissions were measured at the room temperature using a UV/VIS/NIR spectrophotometer (Perkin Elmer LAMBDA 900) in the wavelength range of 600–2,500 nm in 1-nm steps. Raman scattering was performed on a HORIBA LabRAM HR Raman spectrometer at the room temperature. The 633-nm laser line was used as the excitation light source, and the diameter of the laser spot is about 1 μm. Hall Effect and conductivity measurement were carried out on an ET 9003 using the Van Der Paw method. The conductivity of the films was measured in the 50–300 K range. For the electrical measurement, silver-painted electrodes were used as electrical contacts.

3 Results and discussion

3.1 Morphology and composition

Figure 1 shows the surface morphologies and cross-sectional images of the CIGS thin films deposited at different temperatures. A CIGS film, deposited at 200 °C (Fig. 1a), shows pebble-shaped particles homogeneously distributed on the surface. The average size of the particles is in the range of 1–3 μm. The compositions of the particle and the back ground film were determined by EDS, and the results are summarized in Table 1. The EDS results reveal that the grains contain a much higher content of Cu (45.4 at.%) than that of the film (25.7 at.%). The Ga and In contents in the grains are lower. The compositional difference might be correlated to the faster diffusion velocity of copper than that of indium and gallium [12]. As the T_{sub} is elevated to 260 °C, the particles exhibit clear boundary and decreased sizes. The Cu content in the particles decreased significantly, and the Se content increased notably. Meanwhile, a compositional change of the background film is not so obvious. For the films deposited at 320 and 380 °C, Fig. 1c, d shows a uniform and compact morphology, with no particles being distributed on the surface. Both the CIGS films exhibit near-stoichiometric composition. The composition of the 380 °C-deposited film is stoichiometric with $Cu_{23.7}In_{20.8}Ga_{5.8}Se_{49.7}$, which implies a high crystalline quality and a small amount of native defects in the film.

Figure 1e–h denotes the corresponding cross-sectional SEM images of the deposited films. All the CIGS films exhibit compact structure, an no cracks and pinholes can be observed throughout the film. The thickness of the films is about 1 μm. The detailed microstructure from the film

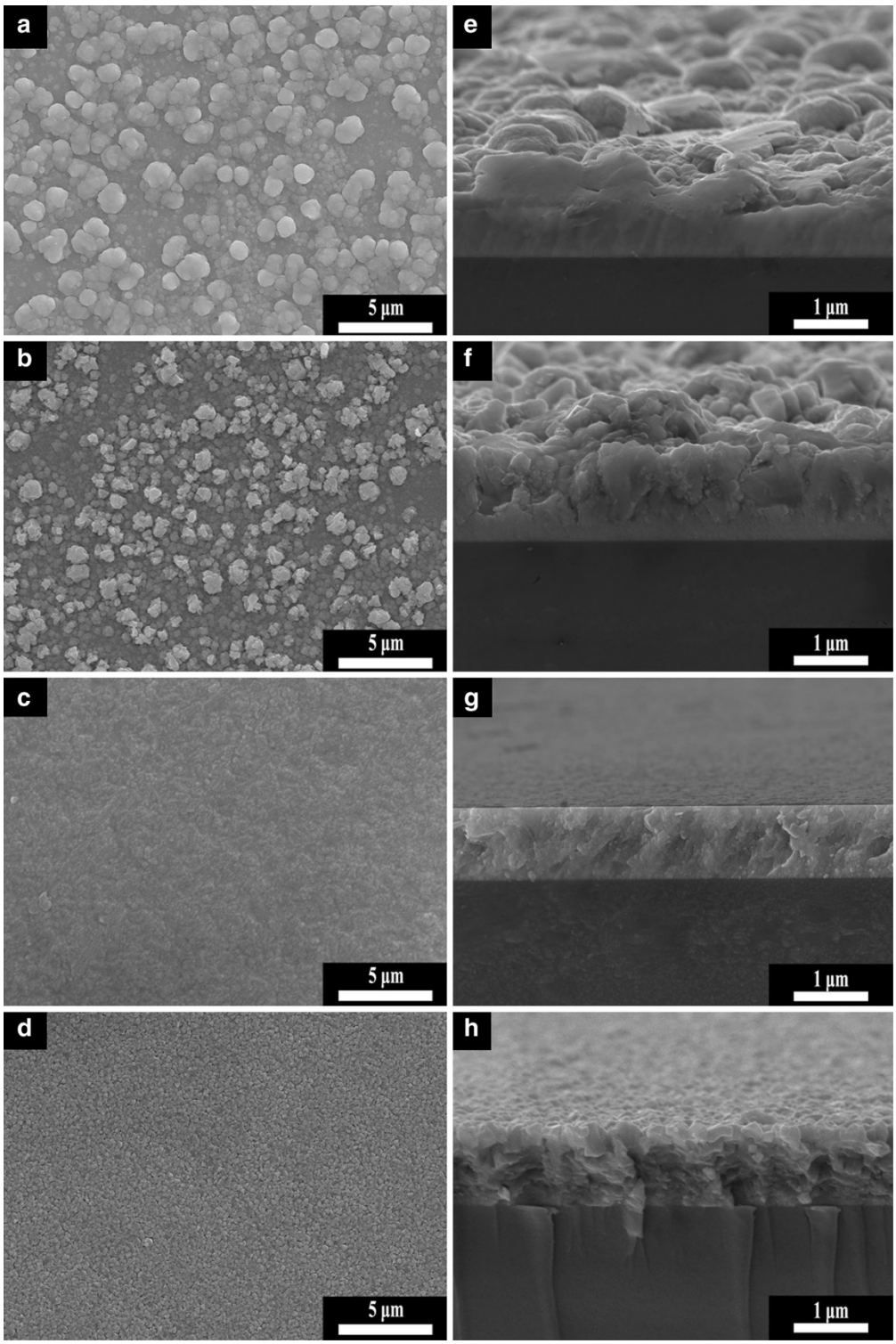

Fig. 1 Top view (**a**–**d**) and cross-sectional (**e**–**h**) SEM images of the CIGS films on glass substrates obtained at various temperatures: 200 °C (**a**, **e**); 260 °C (**b**, **f**); 320 °C (**c**, **g**); and 380 °C (**d**, **h**), respectively

surface down to the bottom can be clearly observed in the SEM cross-sectional images. Figure 1g, h reveals that the 320 °C-deposited film consists of densely packed featureless-shaped grains, and that the 380 °C-deposited film is composed of polyhedral grains with a uniform size of about 200 nm.

Table 1 EDS spectrum of the CIGS film background and particles of the as-deposited film

T_{sub} (°C)	Film						Particles					
	Cu (at.%)	In (at.%)	Ga (at.%)	Se (at.%)	CIG	Se/M	Cu (at.%)	In (at.%)	Ga (at.%)	Se (at.%)	CIG	Se/M
200	25.7	24.5	7.55	42.3	0.80	0.73	45.4	13.4	3.77	37.4	2.64	0.60
260	24.2	21.4	6.73	48.7	0.76	0.95	29.4	14.5	3.24	52.9	1.66	1.12
320	21.8	20.8	6.0	51.3	0.81	1.05	–	–	–	–	–	–
380	23.7	20.8	5.8	49.7	0.89	0.99	–	–	–	–	–	–

CIG is Cu/(In + Ga) ratio, and Se/M is Se/(Cu + In + Ga) ratio

The above results reveal that near-stoichiometric and compact CIGS films can be deposited by the one-step RF sputtering at low T_{sub}. However, the T_{sub} cannot be too low, as at 200 °C, a Cu-rich phase is formed on the film surface. This Cu-rich phase usually acts as recombination center in the CIGS solar cell device and deteriorates the device performance. The Cu-rich phase needs to be removed during the fabricating process of the CIGS solar cell [13].

3.2 Crystal structure

GIXRD patterns of the CIGS films deposited at different T_{sub} are shown in Fig. 2. All the deposited films exhibit three X-ray diffraction peaks located at 26.7°, 44.4°, and 52.8°. These peaks can be indexed to (112), (220)/(204), and (312)/(116) planes of the $CuIn_{0.7}Ga_{0.3}Se_2$ chalcopyrite phase (JCPDS 35-1102), respectively. All GIXRD patterns exhibit a prominent diffraction peak corresponding to CIGS (112) plane. The intensity of the CIGS (112) plane diffraction peak improves with the increasing deposition temperature and reaches its maximum value at 380 °C. From the GIXRD patterns, no other complex peak can be observed in the diffraction angles ranging from 20° to 70°, indicating that no secondary phase can be distinguished by XRD.

The inset of Fig. 2 shows the full width at half maximum (FWHM) values of the CIGS films deposited at various temperatures. As T_{sub} increases, the FWHM value decreases, indicating crystalline quality improvement. Furthermore, the grain size of the film can be calculated using Debye–Scherrer formula:

$$d = \frac{0.94\lambda}{B\cos\theta_B}, \quad (1)$$

where d is the crystalline size, λ is the wavelength of CuKα radiation ($\lambda = 1.54$ Å), B is the FWHM of the (112) peak, and θ_B is the Bragg angle. The calculated grain sizes are 123, 161, and 194 nm for the 260-, 320-, and 380 °C-deposited CIGS films, respectively. It reveals that the crystalline size increases with the elevating T_{sub}.

Raman spectroscopy is considered as an appropriate method to assess the structure of a few material phases, which are difficult to be identified by XRD. Figure 3 depicts

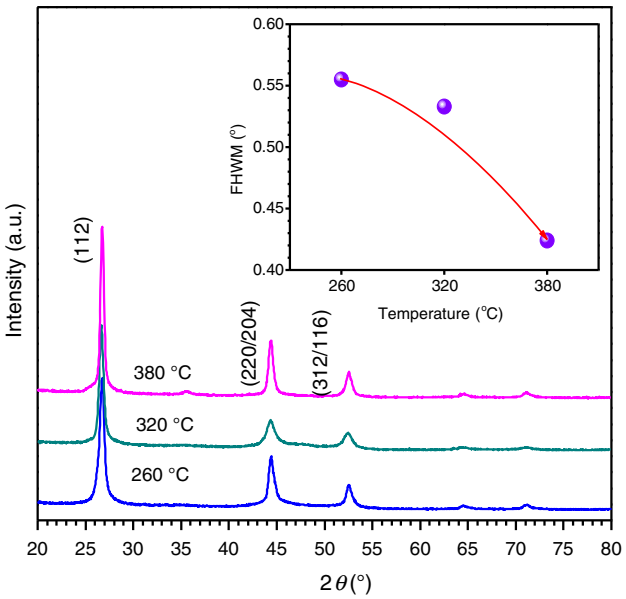

Fig. 2 GIXRD patterns of the CIGS thin films deposited at different temperatures. The inset illustrates the FHWM of (112) peak versus temperature variation

micro-Raman spectra of the deposited CIGS films. All the Raman spectra exhibit a prominent peak located in the range of 175–181 cm^{-1} which corresponds to the A1 mode of the chalcopyrite (CH) CIGS phase. When the T_{sub} is increased, the intensity of A1 vibration peak increases, and the corresponding FWHM value decreases, indicating the improvement of the film crystalline quality. Besides the A1 peak, Raman peaks located at 212 and 229 cm^{-1} can also be observed. These two peaks correspond to the B_2/E and B_2 vibrational modes of the CIGS phase, respectively. The Raman and XRD results both indicate that the low-temperature-deposited CIGS films in this study by one-step RF sputtering exhibit a single-phase polycrystalline chalcopyrite structure without any secondary phases in the films.

3.3 Electrical properties

The resistivity (ρ), conduction type, and carrier concentration of the deposited films were measured using the Van

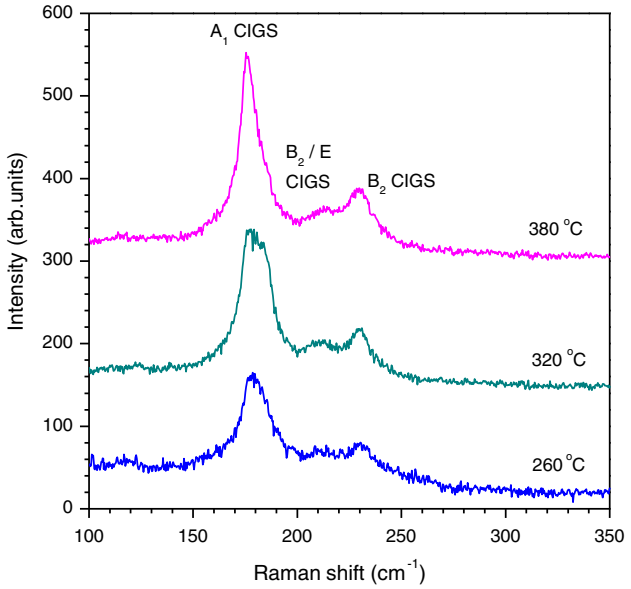

Fig. 3 Raman spectra of CIGS films recorded at room temperature

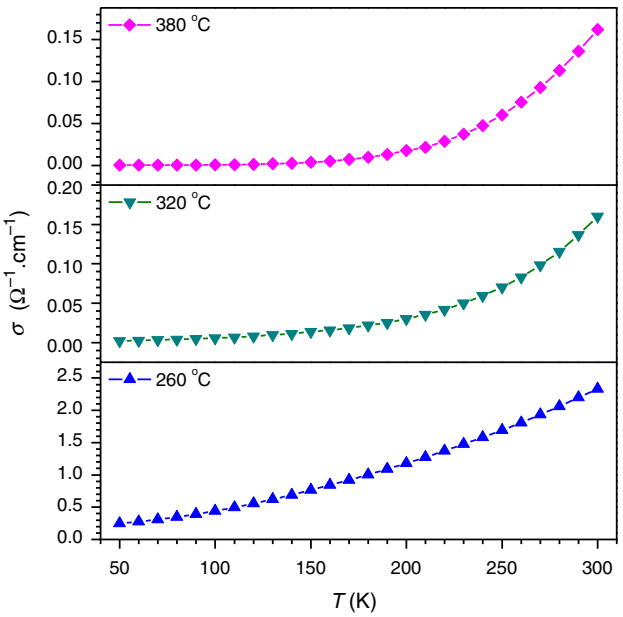

Fig. 4 Temperature dependence of conductivity measurements of the films

Der Paw method at the room temperature [14]. Table 2 summarizes the results obtained from the Hall measurement, which indicates that all the deposited films exhibit *p*-type characteristics. As the T_{sub} is elevated, the resistivity of the film increases, and the carrier concentration is reduced. The resistivity of CIGS films deposited at 320 and 380 °C are suitable for fabricating solar cell devices. Films deposited at 260 °C exhibit a lower resistivity and a higher carrier concentration, which might be attributed to the presence of a Cu-rich phase on the films surface [4].

The temperature (T) dependence of the conductivity (σ) was measured to identify the transport mechanisms in the deposited films. Figure 4 shows that the conductivity of the film increases with the elevating measurement temperature, indicating the semiconducting nature of our CIGS films.

Figure 5 shows the corresponding depicted curves of ln σ versus $10^3/T$ of the deposited CIGS films. The related ln σ versus 1,000/T curves in the temperature range of 50–300 K present two quite different slopes, indicating that the conductivity is affected by two different transport mechanisms. In the high-temperature range (over 120 K), all the curves show linear behavior, indicating a thermionic emission transport mechanism of the films. The activation energy E_a, which determines the potential barrier height, can be calculated from this Arrhenius plots, and it increases from 27 to 90.6 meV as T_{sub} increases from 260 to 380 °C (shown in Table 2). The E_a value of 90.6 meV is very close to that of the CIGS film deposited by three-stage process (98.1 meV) [15]. The E_a value of the 260 °C-deposited film is almost the same as that measured at the room-temperature thermal energy (25.9 meV), which may be attributed to the presence of the trace Cu_2Se phase in the film.

In the low-temperature range of 50–120 K, the curve of σ versus T can be expressed by

$$\sigma = \frac{\sigma_0}{T^{1/2}} \exp\left[-\left(\frac{T_0}{T}\right)^{1/4}\right], \tag{2}$$

where T_0 is the localization temperature, which is associated with the stoichiometry and disorder in the films; and σ_0 is the pre-exponential factor. This conduction process requires a T_0/T ratio much higher than 1. Figure 6 shows the plots of $\ln(\sigma T^{1/2})$ versus $T^{-1/4}$. The plots are

Table 2 Hall effect results of the different CIGS films

T_{sub} (°C)	ρ (Ω·cm)	Carrier concentration (cm^{-3})	P/N	E_a (meV)	T_0 (K)	$N(E_F)$ (cm^{-3})
260	0.438	1.81×10^{18}	P	27.0	7.10×10^4	2.45×10^{19}
320	7.56	7.55×10^{17}	P	73.7	4.47×10^5	3.27×10^{18}
380	8.23	8.97×10^{16}	P	90.6	8.10×10^5	1.74×10^{18}

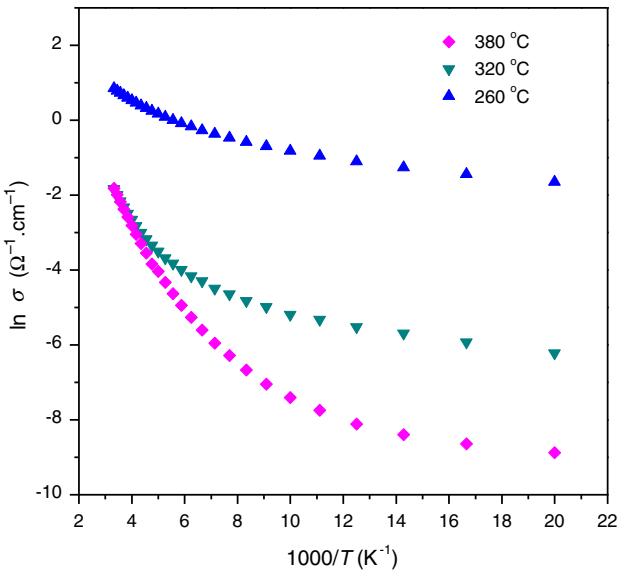

Fig. 5 The depicted curves of ln σ versus $10^3/T$ in the temperature range of 50–300 K

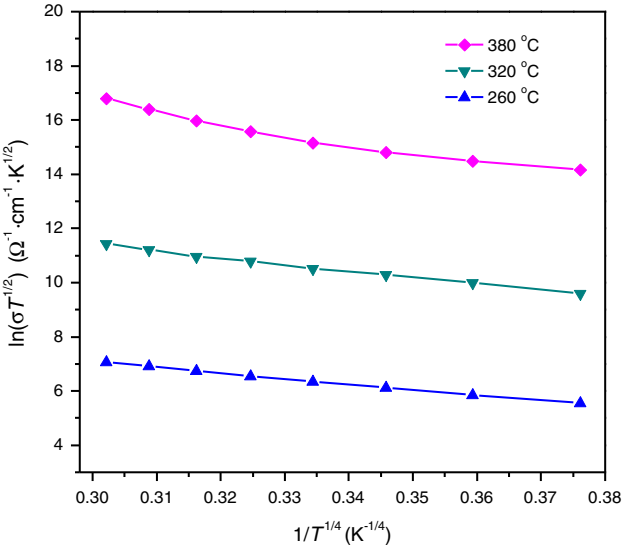

Fig. 6 The depicted curves of $\ln(\sigma T^{1/2})$ versus $T^{-1/4}$ in the temperature range of 50–120 K

linear enough allowing us to interpret the measurements based on our belief that the films are affected by a variable range hopping (VRH) conduction mechanism. As predicted by Davis–Mott model, conductivity is affected by transport in a band of localized states, where the carriers move between states via a phonon-assisted tunneling process [16]. This transport mechanism has already been reported in *n*-type samples of CIGS [17] in Mott's derivation as follows:

$$T_0 = \frac{18\alpha^3}{kN(E_F)}, \quad \text{and } \sigma_0 = 3e^2 v \left(\frac{N(E_F)}{8\pi\eta k}\right)^{1/2}, \tag{3}$$

where $N(E_F)$ is the density of the localized states, k is the Boltzmann constant, η is the decay constant of the wave function of the localized states near the Fermi level, and v is the Debye frequency. The two parameters T_0 and $N(E_F)$ can be evaluated from the slope of $\ln(\sigma T^{1/2})$ versus $T^{-1/4}$ curve and the intercept at $T^{-1/4} = 0$, respectively. Both the T_0 and $N(E_F)$ values are consistent with the proposed model, and they are dominated by T_{sub}. $N(E_F)$ is related to the density of native defects in the films since native defects generate extra energy levels in the forbidden band, forming the localized energy states. Because our 380 °C-deposited film has the stoichiometric composition, the corresponding $N(E_F)$ value is as low as that of the co-evaporated polycrystalline $CuInSe_2$ [18, 19], indicating a low density of the localized state at the Fermi level. Therefore, our low-temperature-deposition method can fabricate CIGS films with the required electrical properties.

3.4 Optical properties

Figure 7 shows the transmittance (T_r) spectra of the CIGS films deposited at various temperatures. Transmittance of the 260 °C-deposited film is kept at a value of 20 % in the range of 1,500–2,400 nm, which might be ascribed to the absorption tails of the Cu-rich particles on the surface [20]. A significant improvement of transmittance and a sharp fall of transmittance at the band edge can be observed when the CIGS films are deposited at a higher temperature. The 380 °C-deposited film exhibits interference patterns in the transmittance spectrum, indicating a very good thickness

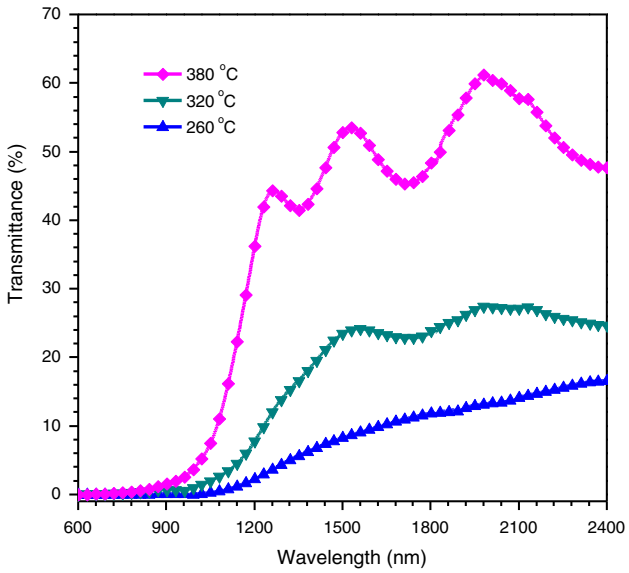

Fig. 7 Optical transmittance of CIGS films as a function of T_{sub}

uniformity of the film, since a small variation of the thickness would destroy the fringe pattern.

For the transmission spectrum with oscillatory patterns, the envelope method (EM) [21] can be used to calculate the refractive index of the film. The envelopes are two curves designated as $T_{\mathrm{r\ max}}$ and $T_{\mathrm{r\ min}}$, which correspond, respectively, the peaks and valleys of the interference patterns in the transparent region of the transmission spectrum. According to the EM, the refractive index, n, is given by

$$n = \left[N + \left(N^2 - S^2\right)^{1/2}\right]^{1/2}, \tag{4}$$

where $N = 2S(T_{\mathrm{r\,max}} - T_{\mathrm{r\,min}})/(T_{\mathrm{r\,max}} \times T_{\mathrm{r\,min}}) + (S^2+1)/2$; S is the refractive index of the substrate; and $T_{\mathrm{r\ max}}$ and $T_{\mathrm{r\ min}}$ are the transmission maximum and the corresponding minimum at a certain wavelength, respectively. The calculated n values at various wavelengths are plotted in Fig. 8. The calculated n values are in the range of 2.61–2.72, which is close to the reported values of single crystal $CuInSe_2$ ($n = 2.9$) and $CuGaSe_2$ ($n = 2.9$) [22]. Figure 7 also reveals the decrease in the refractive index at longer wavelength in the region ranging from 1,700 to 2,200 nm.

The value of absorption coefficient (α) and band gap E_g also can be determined from transmission spectrum as follows:

$$\alpha t = \ln\left(\frac{I_0}{I}\right),\ \alpha h\nu = k\left(h\nu - E_g\right)^{1/2}, \tag{5}$$

where t is the film thickness measured by SEM, I_0 is the incident light intensity, I is the transmitted light intensity,

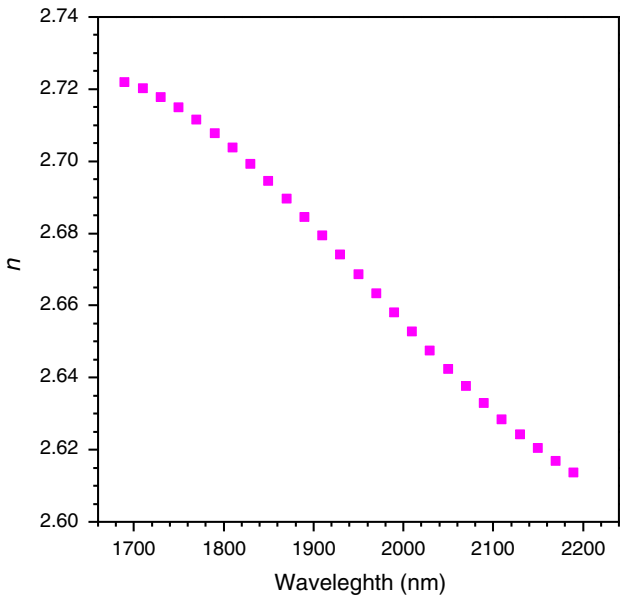

Fig. 8 Refractive index (n) at various wavelengths for the 380 °C-deposited CIGS film

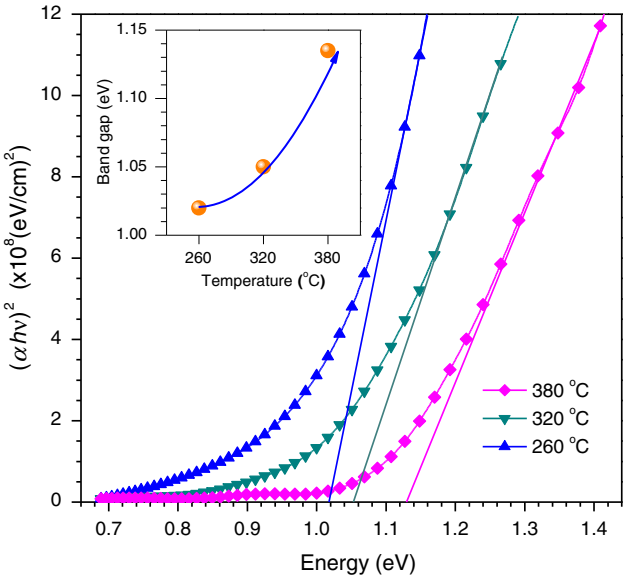

Fig. 9 Plot of $(\alpha h\nu)^2$ versus $h\nu$ for the films deposited at different temperatures. The insert shows the calculated E_g at various T_{sub}

$h\nu$ is photon energy, and k is a constant. Figure 9 shows the relation between $(\alpha h\nu)^2$ and $h\nu$. The linear fit of $(\alpha h\nu)^2$ versus $h\nu$ allows us to obtain the value of E_g. The inset image in Fig. 9 shows the corresponding E_g values; they are in the range of 1.02–1.14 eV and increase with the increasing temperature. Higher temperature reduces the intrinsic defects in the film and results in a smaller amount of energy levels within the forbidden band. Thus, the energy gap between the bottom of conduction band and the top of volume band top increases, enhancing the E_g value. Actually, $E_g = 1.14$ eV for our 380 °C-deposited film is suitable for fabricating solar cell.

4 Conclusion

CIGS films were prepared by a one-step RF magnetron sputtering process at low T_{sub}. It can be concluded that there exists a minimum suitable T_{sub} of 320 °C. Cu-rich particulates are found at less than this temperature. The sample deposited at 380 °C shows near-stoichiometric composition, uniform surface morphology, large grain size (~200 nm), well-crystalline single-phase CIGS. The refractive indexes are in range of 2.61–2.72; the optical band gap is determined to 1.14 eV; and the infrared light transmission is the best. The absorber layer performances depend on T_{sub}, especially the electrical properties.

Acknowledgments The authors gratefully acknowledge the financial supports of the Foundation of National Magnetic Confinement Fusion Science Program (No. 2011GB112001); the Program of International S&T Cooperation (No. 2013DFA51050); the National

Natural Science Foundation of China (No. 51271155, 51377138); and the Science Foundation of Sichuan Province (Nos. 2011JY0031 and 2011JY0130).

References

1. Chopra K, Paulson P, Dutta V (2004) Thin-film solar cells: an overview. Prog Photovolt Res Appl 12(2–3):69–92
2. Repins I, Contreras MA, Egaas B et al (2008) 19.9 %-efficient ZnO/CdS/CuInGaSe$_2$ solar cell with 81.2 % fill factor. Prog Photovolt Res Appl 16(3):235–239
3. Seike S, Shiosaki K, Kuramoto M et al (2011) Development of high-efficiency CIGS integrated submodules using in-line deposition technology. Sol Energy Mater Sol Cells 95(1):254–256
4. Zhang L, Liu F, Li F et al (2012) Structural, optical and electrical properties of low-temperature deposition Cu(In_xGa_{1-x})Se$_2$ thin films. Sol Energy Mater Sol Cells 99:356–361
5. Lammer M, Klemm U, Powalla M (2001) Sodium co-evaporation for low temperature Cu(InGa)Se$_2$ deposition. Thin Solid Films 387(1):33–36
6. Shafarman WN, Zhu J (2000) Effect of substrate temperature and deposition profile on evaporated Cu(InGa)Se$_2$ films and devices. Thin Solid Films 361:473–477
7. Frantz JA, Bekele RY, Nguyen VQ et al (2011) Cu(InGa)Se$_2$ thin films and devices sputtered from a single target without additional selenization. Thin Solid Films 519(22):7763–7765
8. Yu Z, Yan C, Huang T et al (2012) Influence of sputtering power on composition, structure and electrical properties of RF sputtered CuIn$_{1-x}$Ga$_x$Se$_2$ thin films. Appl Surf Sci 258(13): 5222–5229
9. Yu Z, Yan C, Yan Y et al (2012) Effect of annealing temperature on properties of RF sputtered Cu(InGa)Se$_2$ thin films. Appl Surf Sci 258(22):8527–8532
10. Yu Z, Yan Y, Li S et al (2013) Significant effect of substrate temperature on the phase structure, optical and electrical properties of RF sputtered CIGS films. Appl Surf Sci 264:197–201
11. Yu Z, Liu L, Yan Y et al (2012) Properties of different temperature annealed Cu(InGa)Se$_2$ and Cu(InGa)$_2$Se$_{3.5}$ films prepared by RF sputtering. Appl Surf Sci 261:353–359
12. Kim H, Horwitz JS, Qadri SB et al (2002) Epitaxial growth of Al-doped ZnO thin films grown by pulsed laser deposition. Thin Solid Films 420–421:107–111
13. Zhang L, He Q, Jiang W-L et al (2009) Effects of substrate temperature on the structural and electrical properties of Cu(InGa)Se$_2$ thin films. Sol Energy Mater Sol Cells 93(1):114–118
14. Mesa F, Calderón C, Gordillo G (2010) Study of electrical properties of CIGS thin films prepared by multistage processes. Thin Solid Films 518(7):1764–1766
15. Moussa EH, Ariswan GW, Khoury A et al (2002) Fabrication and study of photovoltaic material CuInxGa_{1-x}Se$_2$ bulk and thin films obtained by the technique of close-spaced vapor transport. Solid State Commun 122(3):195–199
16. Essaleh L, Wasim SM (2006) Magnetoresistance and hall mobility in the variable range hopping regime in n-type CuInSe. AIP Conf Proc 850:1470–1471
17. Amara A, Ferdi A, Drici A et al (2006) Electrical and optical study of Cu(InGa)Se$_2$ co-evaporated thin films. Catal Today 113(3): 251–256
18. Gandotra VK, Ferdinand KV, Jagadish C et al (1986) Effect of excess copper on the electrical properties of polycrystalline thin films of CuInSe$_2$. Physica Status Solidi (a) 98(2):595–603
19. Naoki K, Takayuki N, Mikihiko N (1995) Wada takahiro preparation of device-quality Cu(InGa)Se$_2$ thin films deposited by co-evaporation with composition monitor. Jpn J Appl Phys Part 2 34:L1141–L1144
20. Manifacier JC, Gasiot J, Fillard JP (1976) A simple method for the determination of the optical constants *n*, *k* and the thickness of a weakly absorbing thin film. J Phys E 9(11):1002–1004
21. Alonso MI, Wakita K, Pascual J et al (2001) Optical functions and electronic structure of CuInSe$_2$, CuGaSe$_2$, CuInS$_2$, and CuGaS$_2$. Phys Rev B 63(7):075203
22. Park KC, Ma DY, Kim KH (1997) The physical properties of Al-doped zinc oxide films prepared by RF magnetron sputtering. Thin Solid Films 305(1):201–209